Title	Solution characterization of a hyperbranched polysaccharide carbamate derivative and specific phase separation behavior due to chain branching
Author(s)	Mizuguchi, Madoka; Umeda, Keisuke; Mizumoto, Hisato et al.
Citation	Soft Matter. 2023, 19(40), p. 7781-7786
Version Type	AM
URL	https://hdl.handle.net/11094/92805
rights	Reproduced from Soft Matter., 2023, 10, 7675-7860 with permission from the Royal Society of Chemistry.
Note	

Solution characterization of a hyperbranched polysaccharide carbamate derivative and specific phase separation behavior due to chain branching[†]

Madoka Mizuguchi,[a] Keisuke Umeda,[a] Hisato Mizumoto,[a] and Ken Terao*[a]

[a] *Department of Macromolecular Science, Graduate School of Science, Osaka University, 1-1 Machikaneyama-cho, Toyonaka, Osaka 560-0043, Japan*

* Corresponding Author.

E-mail address: terao.ken.sci@osaka-u.ac.jp

[†] Electronic supplementary information (ESI) available.

ABSTRACT

A hyperbranched polymer consisting of rigid helical part chains was prepared as highly branched cyclic dextrin tris(phenylcarbamate) (HTPC) with the weight-average molar masses of 880 and 590 kg mol^{-1}. Small-angle X-ray scattering (SAXS) measurement and viscometry were performed on the samples in good and poor solvents to determine the dimensional and hydrodynamic properties in solution. The HTPC molecule has much more compact conformation than the linear chain with the same molar mass as expected for the hyperbranched architecture. While the corresponding linear polymer is soluble in methyl acetate (MEA) over a wide temperature range, HTPC is only soluble in the solvent at low temperatures. A typical LCST-type phase diagram was observed for the HTPC-MEA system, indicating that the interactions between the polymer segment of HTPC and the MEA molecules are substantially different from those of the linear chains. This is most likely due to the bending helical chains near the branching point of HTPC having different interactions with solvent molecules.

Key Words: hyperbranched polymers; polysaccharide derivative; LCST; small-angle X-ray scattering; viscometry

1. Introduction

Phase separation of polymer solutions is often observed even though the corresponding monomer is well soluble in the solvent due to the low mixing entropy of polymer solutions. This is well expressed by the mean-field approximation theory while the chain architecture is generally difficult to be considered. Experimentally, nonlinear flexible polymers including randomly branched,[1] star,[2-6] and ring polymers,[7, 8] have a wider one-phase region compared to the corresponding linear polymer with the same molar mass. Namely, nonlinear polymers have somewhat better solubility than the linear chain. This tendency is also found for the polymers with more complex architectures.[9] This can be used for the separation of linear and branched polymers.[10]

Phase separation behavior is also found for semiflexible polymers, phenylcarbamate derivatives of cellulose and amylose.[11-13] Although there is little research on the phase separation behavior of semiflexible nonlinear polymers, cyclic amylose tris(n-butylcarbamate) has an appreciably positive second virial coefficient in the theta solvent of the linear chain,[14] meaning that the solubility of the cyclic polymer in the solvent is better than that of the corresponding linear chain. This is consistent with the flexible ring polymers.[15-17] On the contrary, we found that cyclic amylose tris(phenylcarbamate) (cATPC) has a negative second virial coefficient in the theta solvent of linear amylose tris(phenylcarbamate) (ATPC),[18] indicating that the intermolecular interactions between the strained helices of the rigid cyclic cATPC chains via solvent molecules are different from those of the linear chain.[19]

Highly branched cyclic dextrin (HBCD), which was developed by Takata et al.[20, 21] is an amylopectin-based polysaccharide that has a relatively narrow molar mass distribution. We have recently prepared a 3,5-dimethylphenylcarbamate derivative of HBCD (HDMPC)[22] which was only soluble in good solvents. The chiral column made of HDMPC has a somewhat different chiral separation ability compared to the corresponding linear chain, suggesting that

the branching structure can cause the intermolecular interactions between HDMPC and small molecules. A similar trend in chiral separability was also found for the octadecylcarbamate derivative of HBCD.[23] As a preliminary synthesis of the phenylcarbamate derivative of HBCD (HTPC), we found that the solubility of HTPC in some solvents was much worse than that of ATPC and cATPC even though the chemical structure of the part chain of HTPC, ATPC, and cATPC is the same except for the chain ends and branching points as illustrated in Fig. 1, where panel b was illustrated by the same method reported elsewhere.[24] Similar tendency has not been reported to our knowledge while phenylcarbamate derivatives of branched polysaccharides were synthesized.[25, 26] The high bulkiness around the branching point may perturb the local helical structure as well as the intermolecular interactions of HTPC. We thus investigated the molecular shape and phase separation behavior of HTPC in good and poor solvents by small angle X-ray scattering, viscometry, infrared adsorption, circular dichroism, and turbidity measurements.
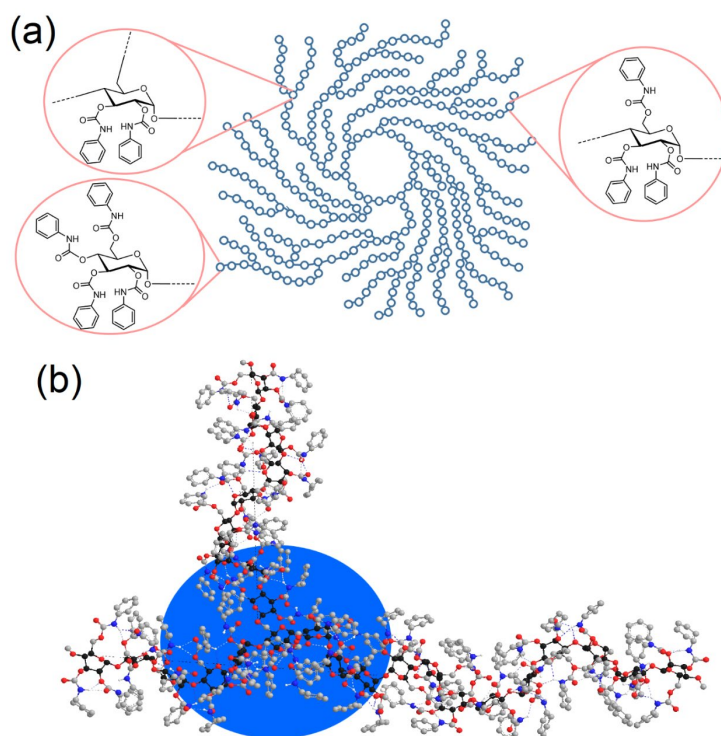

Fig. 1. Chemical structure of HTPC (a) and schematic image of the branching point (b).

2. Experimental section

2.1. Samples

Two HTPC samples were prepared in the manner reported previously for ATPC[27] and hyperbranched cyclic dextrin tris(3,5-dimethylphenylcarbamate)[22] from a reagent grade HBCD (Fujifilm-Wako) sample. The HBCD sample was dissolved into dry dimethylacetamide (Wako) containing lithium chloride under an argon atmosphere. Pyridine (Wako) distilled over CaH_2 and an excess amount of phenyl isocyanate (Wako) were added to the mixture and stirred at 95 °C for 3 h. The crude sample was purified by reprecipitation into methanol. The dried solid sample was redissolved in acetone and reprecipitated into methanol again. For the HTPC sample, fractional precipitation with acetone as solvent and methanol as precipitant was carried out to further purify the HTPC sample to obtain two samples, **HTPC880k** and **HTPC590k**. Ultimate analysis, ^{1}H NMR (400 MHz), and FT-IR (ATR) measurements were carried out to confirm the chemical structure of the samples. The degree of substitution (DS) of the samples was estimated from the weight ratio of nitrogen to carbon to be 2.7 and 3.4 for **HTPC880k** and **HTPC590k**, respectively, indicating full substitution (DS = 3). It should be noted that the branching structure does not influence the DS value, since the number of branching points is essentially the same as that for the non-reducing termini. The ^{1}H NMR spectra in acetone-d_6 at 25 °C in Fig. S1 in the ESI† and the FT-IR spectra in Fig. S2 in the ESI† are consistent with the chemical structure of the previously studied ATPC samples,[27] while the ^{1}H NMR signals are very small probably due to the lower mobility of the HTPC molecules having hyperbranched architecture.

2.2. Measurements of dilute solution properties

SEC-MALS measurements were examined for the samples in THF to determine the

weight-average molar mass M_w and molar mass dispersity using a DAWN DSP multi-angle light scattering photometer (Wyatt) and a RI-4030 refractive index detector (Jasco). A Shodex guard column KF-G 4A and a Shodex SEC column KF-G-806M connected in series and installed in a column oven at 40 °C were used with a flow rate of 0.5 mL min^{-1}. The injection volume was controlled by the sample loop of 100 μL. The wavelength λ_0 in a vacuum of the MALS detector was 633 nm. The specific refractive index increment of HTPC was determined by a modified Schulz-Cantow type refractometer to be 0.180 cm^3 g^{-1} at λ_0 = 633 nm. The obtained chromatogram and molar mass at each elution volume are shown in Fig. S3, ESI†. Since the evaluated data at the two concentrations are substantially similar, we chose the molar mass values calculated from the data of the lower concentration.

Small-angle X-ray scattering (SAXS) measurement was carried out for **HTPC880k** in 1,4-dioxane (DIOX) at 25 °C and methyl acetate (MEA) at −10 °C at the BL40B2 beamline in SPring-8 (Hyogo, Japan). The incident X-ray intensity with λ_0 = 0.1 nm was detected at the lower end of the sample cell to calibrate both the intensity fluctuation and the transmittance. The sample-to-detector distance and the accumulation time were chosen to be 4.2 m and 180 sec, respectively. The circular averaging software SAngler[28] with the silver behenate as the calibrant was used to evaluate the scattering intensity as a function of the magnitude q of the scattering vector. The excess scattering intensity $\Delta I(q)$ was evaluated as the scattering intensity difference between the solution and the solvent with the same quartz capillary cell of 2 mmϕ. The q dependence of $\Delta I(q)$ was analyzed in terms of the square-root Zimm plot (Berry plot, Fig. S4, ESI†) to evaluate the form factor $P(q)$ and the radius of gyration R_g.

Dilute solution viscosity was measured for the two HTPC samples in DIOX at 25 °C and MEA at 5 °C using a Ubbelohde type viscometer. Four solutions with different polymer mass concentrations, c, ranging from 5 to 20 mg mL^{-1} were chosen for this study, resulting in specific viscosities ranging from 0.1 to 0.6. The Huggins and Mead-Fuoss plots were used to

evaluate the intrinsic viscosity $[\eta]$.

Infrared absorption measurement was made for **HTPC880k** in DIOX at 25 °C using a Jasco FT/IR-4200 spectrometer to determine the molar absorption coefficient ε as a function of wavenumber. A solution cell made of CaF_2 with a path length of 0.025 mm was used for the solution with c being 10 mg mL^{-1} and the solvent.   It should be noted that MEA solution was not used because of the significant absorption around the amide I band of the HTPC sample.

Circular dichroism (CD) measurements were made for the HTPC samples in DIOX using a Jasco J720WO CD spectropolarimeter to evaluate the molar circular dichroism $\Delta\varepsilon$. A rectangular quartz cell of 1 mm path length was placed in a thermostatic cell holder.

2.3. Phase separation experiments

Since the HTPC sample was soluble in MEA only at low temperature, the turbidity measurement of the HTPC samples in MEA was examined using a Jasco V750UV/VIS spectrometer with a Peltier temperature controller. A rectangular quartz cell with a path length of 2 mm was placed in a thermostatic cell holder. Optical transmission was observed at $\lambda_0 = $ 550 nm in a vacuum with increasing temperature at a constant heating rate of 0.5 °C min^{-1}.

3. Results and discussion

3.1. Molar masses and conformational properties in dilute solution.

The weight average molar mass M_w and the molar mass dispersity $Đ$, defined as the ratio of M_w to the number average molar mass, were evaluated from the SEC-MALS measurements. The values of M_w and $Đ$ are summarized in Table 1 along with the radius of gyration R_g and intrinsic viscosity $[\eta]$ for the HTPC samples in the two solvents. Their molar mass dependences are plotted in Fig. 2 together with the literature values for linear ATPC at

25 °C.[12, 27] It should be noted that the lower temperatures for HTPC in MEA were chosen because of the LCST-type phase separation behavior, as described later, while the same temperature, 25 °C, was chosen for the DIOX solutions. The evaluated experimental values for the dimensional and hydrodynamic properties of HTPC are much smaller than those for the linear ATPC with the same molar mass, which is consistent with the hyperbranched architecture as in the case of the 3,5-dimethylphenylcarbamate derivative (HDMPC).[22] The radius of gyration contraction factor g_s defined as $R_{g,br}^2/R_{g,lin}^2$ and the intrinsic viscosity contraction factor g_η defined as $[\eta]_{br}/[\eta]_{lin}$ for HTPC in DIOX are calculated and summarized in Table 1 using the same method described elsewhere,[22] where the subscripts br and lin indicate linear and branched chains, respectively. These values are similar to those for HDMPC in methyl acetate, where the chain stiffness is similar to that of HTPC.[22] Both R_g and $[\eta]$ values in MEA are appreciably smaller than those in DIOX, probably reflecting both the poorer solvent quality and the lower chain stiffness in MEA than those in DIOX.
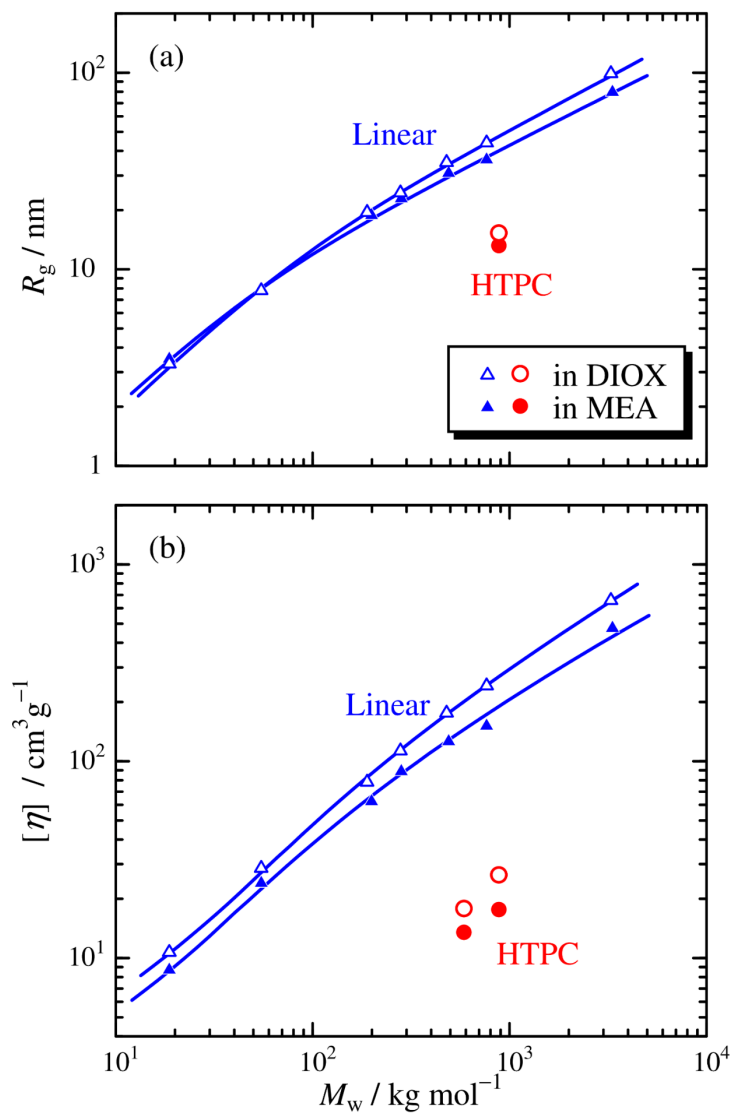
Fig. 2. Weight-average molar mass M_w dependence of (a) the radius of gyration R_g and (b) the intrinsic viscosity $[\eta]$ for the HTPC samples in DIOX at 25 °C (unfilled circles) and in MEA (filled circles) at −10 °C (R_g) or 5 °C ($[\eta]$). Unfilled and filled triangles, literature data for linear ATPC in DIOX[27] and MEA[12] all at 25 °C.

Table 1

Molecular Characteristics of HTPC samples

Sample	M_w / kg mol^{-1}	Đ	Solvent	$[\eta]$ / mL g^{-1}	g_η	R_g / nm	g_s	d *a*	$R_{g,HB}$ / nm *a*
HTPC880k	883	1.65	DIOX	26.7	0.099	16.7	0.124	1.8	17.0
			MEA	17.6		14.1		2.0	14.0
HTPC590k	587	1.49	DIOX	17.8	0.089				
			MEA	13.5					

a: Model Parameters for eq 1.

The high segment density of HTPC samples than that of ATPC can be found more clearly in the form factor $P(q)$ obtained from the SAXS measurement. Fig. 3 illustrates the double logarithmic plots of $P(q)$ vs q for **HTPC880k** in the two solvents. The steep slope of −2.7 and −2.9 for DIOX and MEA solutions, respectively, in the middle q range indicated by the dot-dashed line in each figure cannot be seen for linear flexible and semiflexible polymer chains; the slope value should be between −1 and −2 except for the low-q end, that is the Guinier region. In fact, theoretical dashed curves calculated for the same molar mass linear ATPC using the literature parameters[12, 27] differ significantly from the experimental data for the HTPC sample. Here, we compare the experimental $P(q)$ data with the calculated $P(q)$ for the hyperbranched chain model with the intramolecular excluded volume effect,[29] which was used for some hyperbranched polymers.[30, 31] In this theory, the excluded volume effects are accounted for by the fractal dimension d of the linear flexible chain. The d value for the unperturbed Gaussian chain is 2.0 and that for the good solvent limit is 1.7. The resulting expression is as follows,[29]

$$P(u) = \left[\frac{\sin[(d-1)\arctan(\zeta_{br}u)]}{(d-1)(\zeta_{br}u)(1+\zeta_{br}^2u^2)^{(d-1)/2}}\right]^2 \Bigg/ \left[\frac{\sin[(d-1)\arctan(\zeta_{lin}u)]}{(d-1)(\zeta_{lin}u)(1+\zeta_{lin}^2u^2)^{(d-1)/2}}\right] \quad (1)$$

with

$$\zeta_{br}^{2} = \frac{C+1}{d(d+1)} \qquad (2)$$

$$\zeta_{lin}^{2} = \frac{2C}{d(d+1)} \qquad (3)$$

where $1/C$ and u are the number of branching points and the reduced scattering vector defined by $u = q\, R_{g,HB}$ with $R_{g,HB}$ being the gyration radius of the hyperbranched chain. Since the number-average repeat unit of α-1,6-linkage hydrolyzed HBCD was estimated to be 16,[20, 21] the $1/C$ value was estimated from $N_w/16 = 106$ where N_w is the weight average degree of polymerization. A curve fitting procedure was employed for the $P(q)$ data to estimate the remaining two parameters, $R_{g,HB}$ and d. The resulting theoretical values, shown as solid curves in Fig. 3, mostly reproduce the experimental data except for the high q region. A similar discrepancy has also been reported for the HBCD 3,5-dimethylphenyl carbamate derivative[22] and hyperbranched aliphatic-aromatic polyesters,[30] suggesting the contribution from the monomeric unit. In fact, the calculated $P(u) + 1/N_w$ values fairly explain the experimental data (not shown here). It is noted that the Kratky plot shown inlet in each figure was also utilized to find the best fit curve. The evaluated $R_{g,HB}$ values are substantially the same as R_g, thus reasonable. Indeed, the theoretical values plotted in the Berry plot in Fig. S4 excellently reproduce the experimental data. The fractal dimension d values in DIOX and MEA are consistent with good solvent and theta solvent systems, respectively.
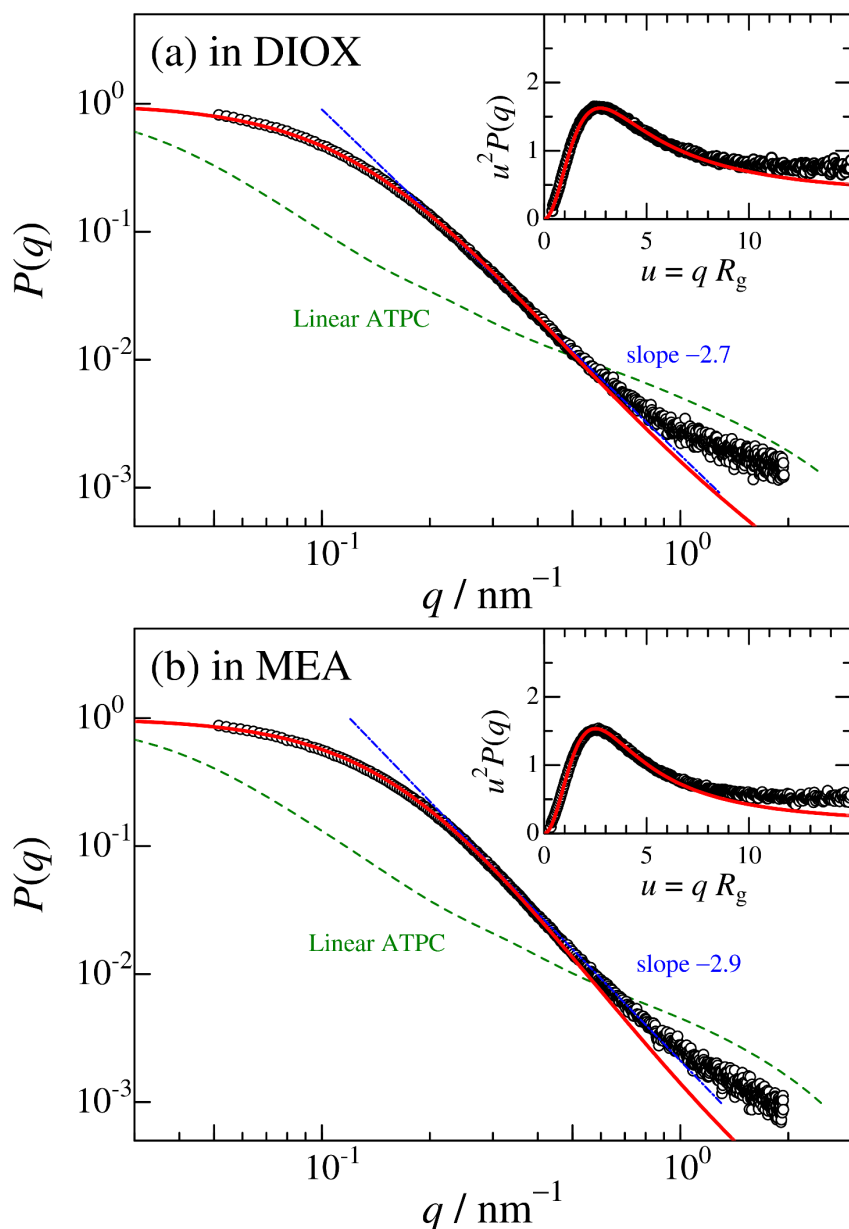
Fig. 3. Double logarithmic plots of the form factor $P(q)$ vs q for **HTPC880k** (unfilled circles) in DIOX at 25 °C (a) and in MEA at −10 °C (b). The inset of each panel is the Kratky plot. Solid red curves denote the theoretical values from Eq. 1.

Fig. 4 shows the IR spectra for **HTPC880k** in DIOX along with that for a previously investigated linear ATPC sample (**ATPC300K**, $Đ = 1.09$).[27] The bimodal amide I band shown between 1700 and 1760 cm^{-1} indicates that a certain amount of carbonyl groups form a hydrogen bond with the NH group on the adjacent glucose unit. It should be noted that

interchain hydrogen bonding is insignificant, as essentially no concentration dependence of the IR spectra was observed for linear ATPC.[27] While the higher peak at 1753 cm^{-1} for HTPC, reflecting free C=O groups, is essentially the same as that for ATPC, another peak for intramolecular hydrogen bonding C=O groups is slightly different for the two polymers. This suggests that the average local helical structure of HTPC is somewhat different from that of ATPC, at least near the branching point, due to the high bulkiness around the branching point shown in Fig. 1. Note that the difference is not sufficiently large to influence the circular dichroism, as shown in Fig S5, where the CD spectra for **HTPC880k** and **HTPC590k** are substantially fitted by the experimental CD spectra for previously studied linear and cyclic ATPC samples.[27, 32]
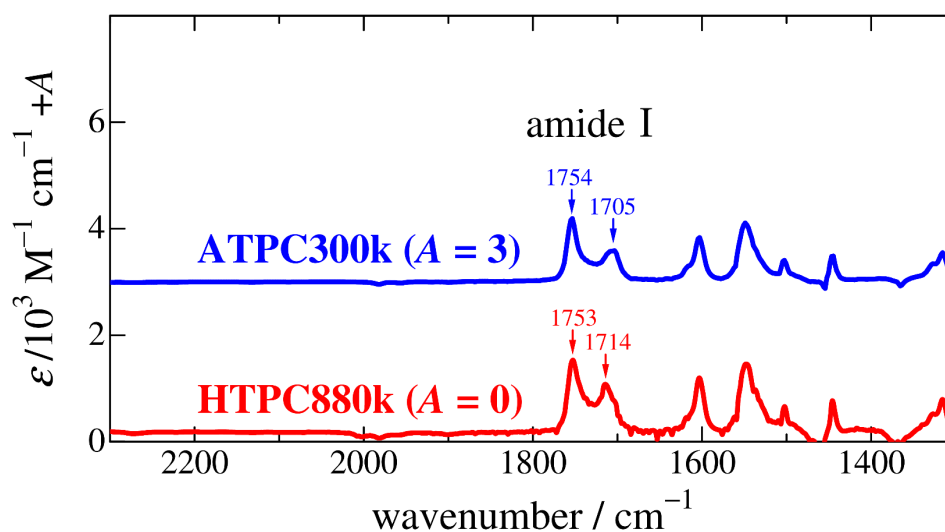
Fig. 4. IR spectra for **HTPC880k** in DIOX at 25 °C along with that for **ATPC300K**.[27] The ordinate values are shifted by A.

3.2. LCST phase separation behavior of HTPC in MEA.

In general, although branched polymers have similar or somewhat better solubility than the linear polymers, the HTPC samples were not soluble in ethyl acetate and 4-methyl-2-pentanone which are LCST-type theta solvents for linear ATPC.[12] MEA is also a theta solvent for ATPC while the phase separation temperature is much higher than that for HTPC. In fact, high molar mass linear ATPC samples are soluble in MEA at 25 °C, and therefore the dimensional and hydrodynamic properties were determined as shown in Fig. 2. In contrast, HTPC is only soluble in MEA at low temperatures. We therefore estimated the phase diagram using the cloud point temperature. Fig. 5a displays the temperature dependence of the transmittance for **HTPC880k** in MEA at a heating rate of 0.5 °C min^{-1}. The temperature at which the transmittance decreased to 90% of the initial value was defined as the cloud point temperature T_c. The resulting cloud point curves for the two HTPC samples are shown in Fig. 5b. Although the data points are scattered, the cloud point temperature tends to rise with increasing c, suggesting that the critical point of LCST-type phase separation is in the concentration range investigated. The critical temperature is roughly estimated to be 10 °C ± 5 °C. This significantly lower solubility of HTPC than that of ATPC is most likely due to the different helical structure, as suggested by the solution IR spectra, because NH groups of HTPC (or ATPC) tend to form hydrogen bonds with the carbonyl group of MEA, but the hydrogen bonding structure can be influenced by the local helical structure considering that the polar NH groups are located in the narrow space between the main chain and the phenyl groups. It should be noted that the chain end effect may not be significant for the intermolecular interactions, because the second virial coefficient for short linear ATPC, for which the degree of polymerization is 36 and 106, mostly disappeared; this was estimated from our previous SAXS data.[12] Although the difference in phase separation behavior between linear and branched polymers cannot be explained by the mean-field theories, we may consider that the difference in polymer-solvent interactions cause the significantly lower solubility of HTPC in MEA, and

also in ethyl acetate and in 4-methyl-2-pentanone. Indeed, an appreciably smaller second virial coefficient has been reported for cyclic ATPC,[18] for which the local helical structural difference from the corresponding linear chain can be observed from the SAXS data.
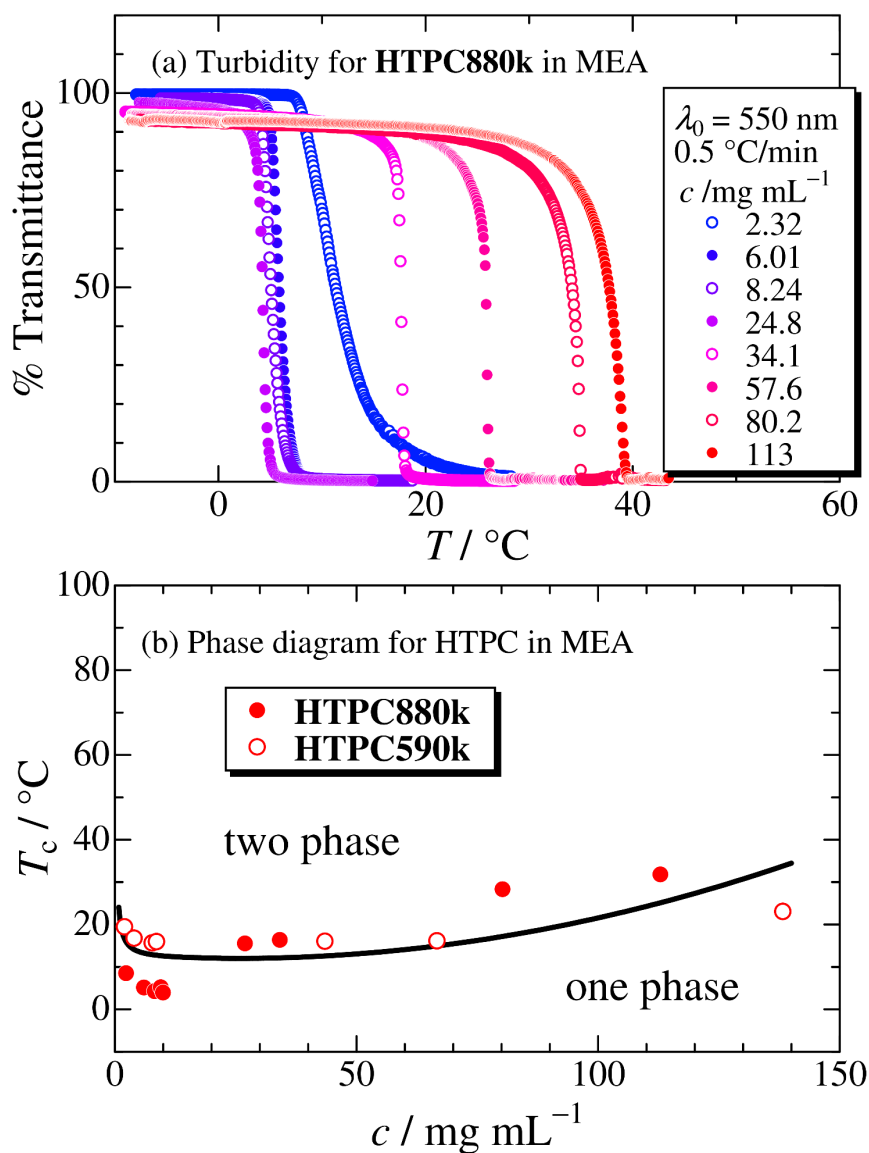

Fig. 5. (a) Results of the turbidity measurement for **HTPC880k** in MEA and (b) cloud point curves for the indicated HTPC samples in MEA.

4. Conclusion

We have successfully prepared two samples of hyperbranched amylose phenylcarbamate derivative, that is, highly branched cyclic dextrin tris(phenylcarbamate) (HTPC). The dimensional and hydrodynamic properties in good and theta solvents, 1,4-dioxane and methyl acetate, respectively, are consistent with the hyperbranched structure. Especially, the form factor $P(q)$ can be explained in terms of the known theory for hyperbranched polymers. The intramolecular hydrogen bonding structure between C=O and NH groups of HTPC in 1,4-dioxane is slightly different from that of linear ATPC, suggesting that the distorted helical structure of HTPC owing to the bulky side groups may be located especially around the branching point. Although linear ATPC with high molar mass of $M_w = 3330$ kg mol^{-1} is soluble in MEA with zero second virial coefficient around room temperature,[12] HTPC shows LCST type phase separation behavior below room temperature. The phase diagram was constructed to estimate the critical temperature of 10 °C ± 5 °C, irrespective of the sample. The thermodynamic difference between ATPC and HTPC clearly showed the intermolecular interactions of the polymer chains is significantly affected by the chain branching. Namely, the helical structure and intramolecular hydrogen bonding structure distorted by chain branching significantly influence the polymer-solvent interactions. This study predicts that highly branched polymers consisting of stiff part chains may have significantly different functionality, especially for polymer-small molecule interactions.

Author contributions

M. M.: Investigation, Formal analysis, Writing - Original Draft. K. U.: Investigation, Formal analysis. H. M.: Investigation. K. T.: Conceptualization, Formal analysis, Writing - Original Draft, Writing - Review & Editing, Supervision.

Conflicts of interest

There are no conflicts of interest to declare.

References

1. S. Sato, M. Okada and T. Nose, *Polym. Bull.*, 1985, **13**, 277-284.
2. J. M. G. Cowie, A. Horta, I. J. Mcewen and K. Prochazka, *Polym. Bull.*, 1979, **1**, 329-335.
3. H. Yokoyama, A. Takano, M. Okada and T. Nose, *Polymer*, 1991, **32**, 3218-3224.
4. K. Terao, M. Okumoto, Y. Nakamura, T. Norisuye and A. Teramoto, *Macromolecules*, 1998, **31**, 6885-6890.
5. M. L. Alessi, K. C. Bittner and S. C. Greer, *Journal of Polymer Science Part B-Polymer Physics*, 2004, **42**, 129-145.
6. Y. Tasaka, M. Okumoto, Y. Nakamura and T. Norisuye, *Polym. J.*, 2008, **40**, 634-639.
7. X.-P. Qiu, F. Tanaka and F. M. Winnik, *Macromolecules*, 2007, **40**, 7069-7071.
8. Y. Jung, J. H. Kim and W. D. Jang, *Eur. Polym. J.*, 2017, **88**, 605-612.
9. J. Zhou, J. Yang, M. W. Ishaq and L. Li, *Macromolecules*, 2022, **55**, 1398-1411.
10. S. Boye, L. Scharfenberg and A. Lederer, *J. Sep. Sci.*, 2010, **33**, 3584-3594.
11. W. Burchard, *Polymer*, 1969, **10**, 467-&.

12. T. Fujii, K. Terao, M. Tsuda, S. Kitamura and T. Norisuye, *Biopolymers*, 2009, **91**, 729-736.
13. Y. Sano, K. Terao, S. Arakawa, M. Ohtoh, S. Kitamura and T. Norisuye, *Polymer*, 2010, **51**, 4243-4248.
14. K. Terao, K. Shigeuchi, K. Oyamada, S. Kitamura and T. Sato, *Macromolecules*, 2013, **46**, 5355-5362.
15. J. Roovers and P. M. Toporowski, *Macromolecules*, 1983, **16**, 843-849.
16. J. X. Huang, J. Shen, C. R. Li and D. Z. Liu, *Makromolekulare Chemie-Macromolecular Chemistry and Physics*, 1991, **192**, 1249-1254.
17. A. Takano, Y. Kushida, Y. Ohta, K. Masuoka and Y. Matsushita, *POLYMER*, 2009, **50**, 1300-1303.
18. N. Asano, S. Kitamura and K. Terao, *J. Phys. Chem. B*, 2013, **117**, 9576-9583.
19. K. Terao, A. Ryoki, S. Kitamura and T. Sato, *Macromolecular Symposia*, 2023, **408**, 2200024.
20. H. Takata, K. Ohdan, T. Takaha, T. Kuriki and S. Okada, *Journal of Applied Glycoscience*, 2003, **50**, 15-20.
21. H. Takata, T. Takaha, S. Okada, S. Hizukuri, M. Takagi and T. Imanaka, *Carbohydr. Res.*, 1996, **295**, 91-101.
22. A. Kishimoto, M. Mizuguchi, A. Ryoki and K. Terao, *Carbohydr. Polym.*, 2022, **290**, 119491.
23. A. Kishimoto, A. Ryoki, S. Kitamura and K. Terao, *Polymer*, 2023, **284**, 126303.
24. K. Terao, M. Murashima, Y. Sano, S. Arakawa, S. Kitamura and T. Norisuye, *Macromolecules*, 2010, **43**, 1061-1068.
25. I. A. Wolff, P. R. Watson and C. E. Rist, *J. Am. Chem. Soc.*, 1953, **75**, 4897-4899.
26. R. Helm, R. A. Young, R. Mcpherson and R. Klem, *Carbohydr. Polym.*, 1986, **6**, 443-462.
27. K. Terao, T. Fujii, M. Tsuda, S. Kitamura and T. Norisuye, *Polym. J.*, 2009, **41**, 201-207.
28. N. Shimizu, K. Yatabe, Y. Nagatani, S. Saijyo, T. Kosuge and N. Igarashi, *AIP Conf. Proc.*, 2016, **1741**, 050017.
29. W. Burchard, *Macromolecules*, 2004, **37**, 3841-3849.
30. W. Burchard, A. Khalyavina, P. Lindner, R. Schweins, P. Friedel, M. Wiemann and A. Lederer, *Macromolecules*, 2012, **45**, 3177-3187.
31. E. De Luca, R. W. Richards, I. Grillo and S. M. King, *J. Polym. Sci., Part B: Polym. Phys.*, 2003, **41**, 1352-1361.
32. K. Terao, N. Asano, S. Kitamura and T. Sato, *ACS Macro Lett*, 2012, **1**, 1291-1294.

Solution characterization of a hyperbranched polysaccharide carbamate derivative and specific phase separation behavior due to chain branching

Madoka Mizuguchi,[a] Keisuke Umeda,[a] Hisato Mizumoto,[a] and Ken Terao*[a]

[a]Department of Macromolecular Science, Graduate School of Science, Osaka University, 1-1 Machikaneyama-cho, Toyonaka, Osaka 560-0043, Japan

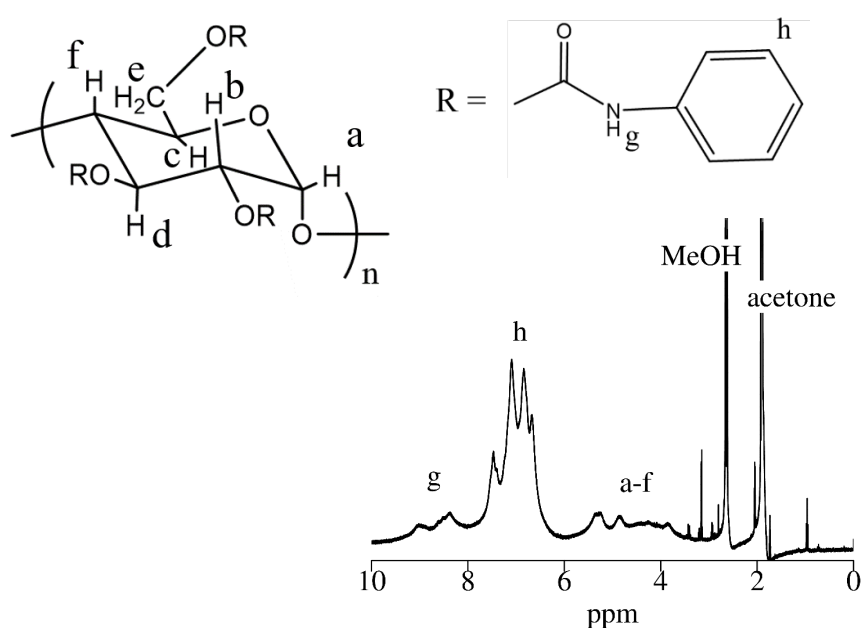* Corresponding author. E-mail address: terao.ken.sci@osaka-u.ac.jp

Fig. S1. ^{1}H-NMR spectrum of **HTPC880k** in acetone-d_6 at 25 °C.
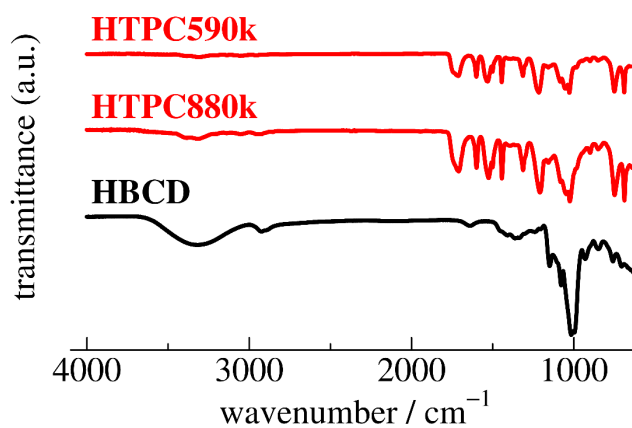
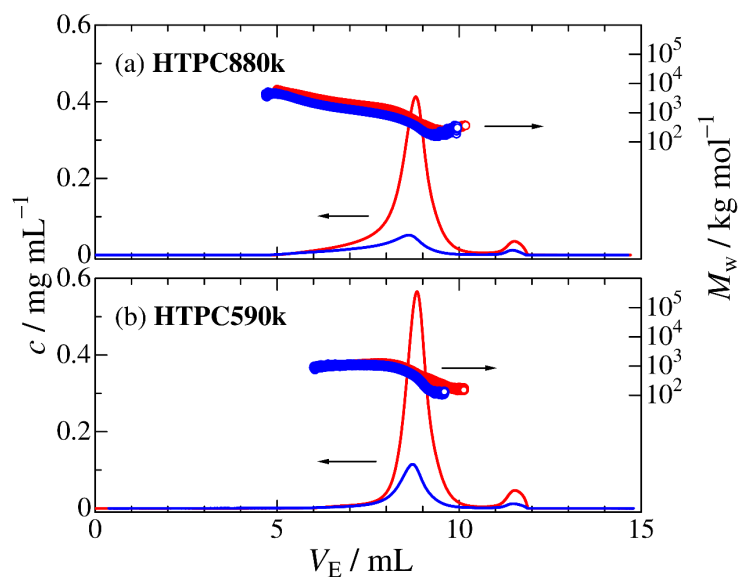**Fig. S2.** FT-IR spectra for the indicated polysaccharide and polysaccharide derivative samples.

Fig. S3. Results of SEC-MALS measurement for **HTPC880k** (a) and **HTPC590k** (b) in THF at 25 °C. Different colored symbols indicate the different concentration of the injected solution. Retention volume V_E dependence of the polymer mass concentration c (blue solid curves) and the weight-average molar mass M_w (red circles).
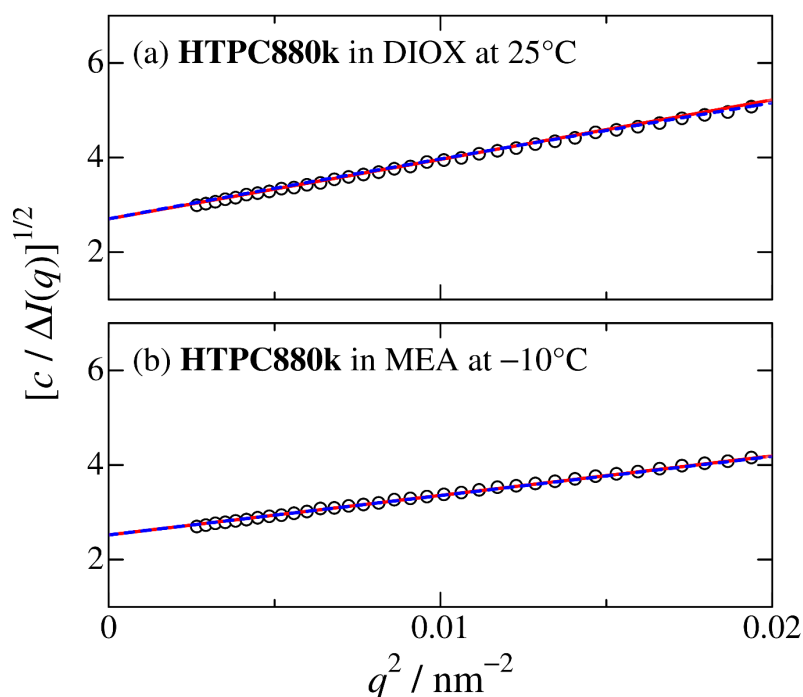

Fig. S4. Berry plots for **HTPC880k** in DIOX at 25 °C (a) and in MEA (b) at −10 °C. $\Delta I(q)$, c, and q are the excess scattering intensity of X-ray, polymer mass concentration, and the magnitude of the scattering vector, respectively. The solid red and dashed blue lines indicate the initial slope to estimate the radius of gyration R_g and the theoretical values calculated from eqs 1-3 in the main text.
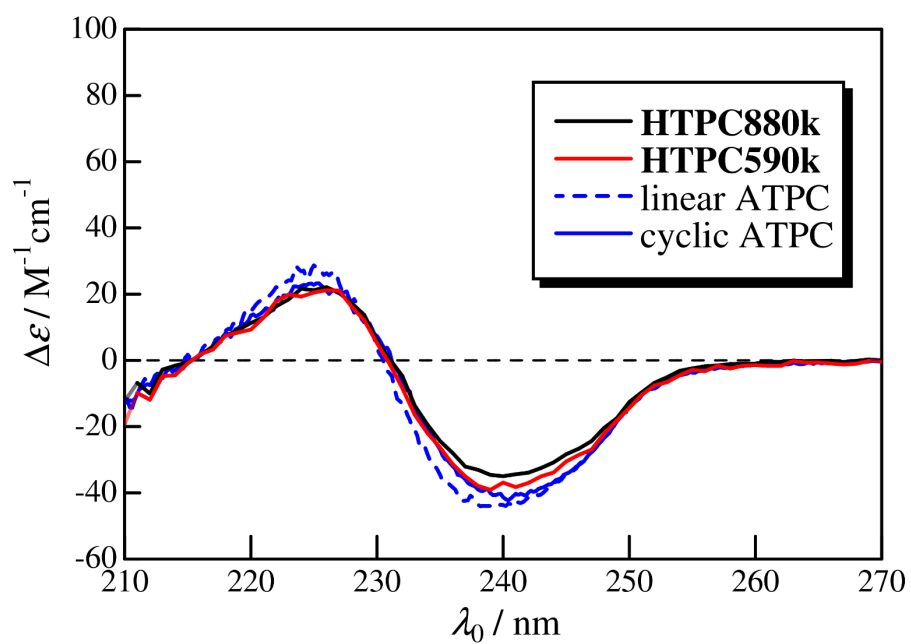
Fig. S5. Circular dichroism spectra for **HTPC880k** and **HTPC590k** in DIOX at 25 °C along with that for linear ATPC[1] and cyclic ATPC.[2]

References

1.   K. Terao, T. Fujii, M. Tsuda, S. Kitamura and T. Norisuye, *Polym. J.*, 2009, **41**, 201-207.

2.   K. Terao, N. Asano, S. Kitamura and T. Sato, *ACS Macro Lett*, 2012, **1**, 1291-1294.